

Vibration control with piezoelectric elements: the indirect measurement of the modal capacitance and coupling factor

M. Berardengo^{1,2}, S. Manzoni³, J. Høgsberg⁴, M. Vanali²

1. *Università degli Studi di Genova - Department of Mechanical, Energy, Management and Transportation Engineering*

Via Opera Pia, 15A - 16145 Genoa, Italy

2. *Università degli Studi di Parma - Department of Engineering and Architecture
Parco Area delle Scienze, 181/A - 43124 Parma, Italy*

3. *Politecnico di Milano - Department of Mechanical Engineering
Via La Masa, 34 - 20156 Milan, Italy*

4. *Technical University of Denmark - Department of Mechanical Engineering
Nils Koppels Allé, building 403
DK-2800 Kongens Lyngby, Denmark*

Abstract

The knowledge of the modal capacitance and electro-mechanical coupling factor is essential for a proper design of systems with embedded piezoelectric transducers and materials. In light of this, this paper presents two indirect methods for measuring the piezoelectric modal capacitance and a method to estimate the modal electro-mechanical coupling factor. All methods rely on simple vibration measurements of the structure with the piezoelectric transducer connected to a proper shunt impedance, thus avoiding measurements of piezoelectric current and voltage by expensive equipment. For the modal electro-mechanical coupling factor, the proposed method guarantees reduced uncertainty compared to traditional experimental estimation procedures. Upon introduction of the underlying theory, the paper experimentally demonstrates the reliability and effectiveness of the methods by comparison with well-established procedures.

Keywords: vibration control, modal capacitance, coupling factor, piezoelectric shunt, negative capacitance, resonant shunt

*marta.berardengo@unige.it

Email address: (M. Berardengo^{1,2}, S. Manzoni³, J. Høgsberg⁴, M. Vanali²)

1 **1. Introduction**

2 Vibration control of structures is a fundamental issue for their durability
3 and performances. This aspect has become even more important in the last
4 decades since many applications rely on lightweight structures subject to a
5 harsh dynamic environment. In these cases, the high vibration level could cause
6 material fatigue, shortening the operating life of the system due to possible
7 damages, and also increase of maintenance costs. Consequently, the reduction
8 of the undesirable vibrations becomes a fundamental issue. In this scenario,
9 piezoelectric materials play an important role because their use does not cause
10 much additional weight, which is a key point for the majority of light structures,
11 they allow to achieve wide control bandwidths and significant forces, they are
12 characterised by low power consumption and can be used both as sensors and
13 actuators and therefore they show attractive features for both active and passive
14 control strategies. Piezoelectric materials have been successfully used for active
15 control in several applications [1], such as in truss structures [2], helicopters [3],
16 spacecrafts [4], satellites [5] and also in civil engineering [6]. A detailed review of
17 recent developments in the field of active vibration control through piezoelectric
18 actuators has been published by Shivashankar and Gopalakrishnan [7].

19 Particular attention has been paid to the optimisation of the control strategy,
20 by e.g. fuzzy-logic algorithms [8], optimal control [9], multi-objective optimiza-
21 tion algorithms [10] or other types of controller [11, 12], the geometrical and ma-
22 terial parameters [13, 14, 15] and the location on the structure to maximise the
23 control effect, while keeping the control effort as low as possible [16]. Different
24 algorithms have been employed for the optimisation of the actuator/sensor posi-
25 tion on complex structures, such as genetic algorithms [17], model-based linear
26 quadratic regulators [18] or other criteria [19, 20]. Optimal configurations have
27 been proposed for different applications, such as the rear wing of a racing car
28 [21] or adaptive trusses [22], and various frequency ranges [23]. The reason why
29 great attention has been paid to these aspects is that the actuation capability

30 depends on the coupling between the strain field and the electrical field [24, 25],
31 represented by the electro-mechanical coupling factor [26] that is a function of
32 the electrical, mechanical and geometrical characteristics of the piezoelectric
33 transducer on the structure [27]. This parameter constitutes the foundation of
34 piezoelectric structural control and its estimation is thus important for a proper
35 control design. This is verified by studies that specifically develop methods for
36 the estimation of the coupling coefficient, such as in Chesne et al. [28] where
37 an approach especially effective for small parameter values is presented. The
38 knowledge of the electro-mechanical coupling factor is as well important in other
39 piezoelectric-based applications, for example in energy harvesting, where an ac-
40 curate estimation of the coupling factor allows for a proper prediction of the
41 effectiveness of the electro-mechanical conversion [29], as further evidenced in
42 e.g. [30, 31].

43 The key role of the coupling factor becomes even more important when pas-
44 sive or semi-passive control is considered, for example in piezoelectric shunt
45 damping [32] or synchronized switch damping [33]. In these cases, the mechan-
46 ical energy, converted into electrical energy, is reused to properly control the
47 structure. Thus, the performances of these strategies strongly depend on the
48 coupling factor, making its estimation essential for effective tuning of the con-
49 trol parameters to maximize the achievable attenuation. Several studies on this
50 topic have been carried out in the field of piezoelectric shunt damping, where the
51 control action is obtained through the connection of a proper electric impedance
52 (shunt) across the piezoelectric transducer electrodes [34, 35], thereby effectively
53 attenuating vibrations in e.g. beams [36] or plates [37]. The control action can
54 be designed for different targets, depending on the type of impedance. The
55 simplest shunt impedances can be composed of a pure resistance [26] or its se-
56 ries/parallel connection with an inductance [38, 39]. The tuning of the shunt
57 impedance can rely on different principles, such as pole placement techniques
58 [40, 41] or minimisation of the system Frequency Response Function (FRF)
59 [42, 43]. Furthermore, multi-branch impedances can be used for multi-mode
60 vibration control, by the current blocking method of Wu [44] or the subsequent

61 current flowing technique proposed by Behrens et al. [45]. Modified versions
62 of these solutions have since been analysed and proposed to improve the pre-
63 vious techniques [46, 47]. More complex networks can be used for broadband
64 [48, 49], non-linear [50, 51] or noise control [52], for control with multiple trans-
65 ducers [53, 54], and in different applications for cable damping [55] and vibration
66 isolation [56]. Moreover, synchronized switch damping aims at enhancing the
67 control performance by adding switches to the shunt circuit, based on active ele-
68 ments [57], inductors [58], voltage sources [33], or even periodic impedances [59].
69 However, in all the above cases, regardless the impedance used and the tuning
70 strategy applied, the accurate estimation of the piezoelectric transducer capaci-
71 tance and coupling factor is required to effectively tune the control system. Up
72 to few years ago, most of the literature relied on models where the value used
73 for the piezoelectric capacitance was the blocked capacitance, associated with
74 the transducer linked to a blocked structure. However, since a thin structure
75 is usually flexible and exhibits significant dynamic behaviour, this piezoelectric
76 capacitance value coincides with the value at infinite frequency, where the dy-
77 namic response of the flexible structure vanishes [60, 61]. Therefore, this value
78 of the capacitance will be referred to as C_∞ .

79 Few years ago, it was observed that the use of C_∞ in reduced order models of
80 the electro-mechanical system is not able to provide accurate tuning of the shunt
81 impedance, resulting in non-optimised attenuation performances. Indeed, to
82 achieve an optimal tuning, a modified value of the piezoelectric capacitance must
83 be used, which accounts for the contribution from the neglected modes to the
84 electrical behaviour of the system. Supposing that the control action is focused
85 on the s -th mode of the system, the capacitance value to be used is the modal
86 capacitance C_s that is obtained by adding a correction term C'_s to C_∞ . The
87 term C'_s allows to take into consideration the influence of the modes higher than
88 the s -th [60, 62]. Moreover, the knowledge of the modal capacitance C_s has been
89 proved to be important for a proper tuning also in case of multi-mode control
90 [63], and not only for single mode control. **Despite the importance of the modal**
91 **capacitance was observed in the field of piezoelectric shunt damping, it plays the**

92 same significant role when dealing with active control or energy harvesting since
93 it allows for a more accurate description of the electro-mechanical structure.

94 Since then, different methods have been proposed in the literature to esti-
95 mate the modal capacitance. Berardengo et al. [64] proposed to measure the
96 trend of the capacitance of the piezoelectric patch as a function of the frequency
97 and then to fit the experimental data with a model. Toftekær and Høgsberg [65]
98 developed a method based on the measurement of modal charge and voltage.
99 The two methods are based on the same model of the system and thus lead to
100 similar results. Even if the two methods are effective in estimating C_s , both re-
101 quire to measure the current flowing through the piezoelectric transducer. Since
102 this current is very low, dedicated hardware is needed to carry out a reliable
103 measurement, often with the need of expensive impedance analyzers.

104 To overcome this issue, this paper proposes two alternative methods that
105 allow for an indirect measurement of the modal capacitance C_s . Both are based
106 on the use of simple and inexpensive hardware that is usually present in labs
107 where vibration measurements are performed (e.g. low-cost accelerometers),
108 common acquisition boards and additional inexpensive electronic devices.

109 Furthermore, taking advantage of the theory behind one of the two methods
110 proposed for the estimation of the modal capacitance, a new method to derive
111 the modal electro-mechanical coupling factor is presented in this paper. As
112 mentioned, the importance of this parameter in piezoelectric control is well
113 known because it is an index of the energy transfer between the electrical and
114 mechanical parts of the system (e.g. [24]) and several studies focused on its
115 estimation via analytical (e.g. [27]), numerical (e.g. [66]) and experimental (e.g.
116 [24, 25]) methods. In general, and especially for complex structures, the most
117 reliable and easy-to-apply experimental procedure is based on the estimation
118 of the short- and open-circuit eigenfrequencies (i.e. with the terminals of the
119 piezoelectric transducer short- and open-circuited, respectively). However, if
120 these two frequencies are really close to each other (i.e. either due to small
121 values of the modal electro-mechanical coupling factor or because the considered
122 mode is at low frequency), the estimation of this coupling coefficient can be

123 significantly affected by the uncertainty on the estimates of the two mentioned
 124 eigenfrequencies. The method proposed in this paper is shown to provide an
 125 estimate of the coupling coefficient with a reduced uncertainty level compared
 126 to the traditional experimental method and, therefore, to provide more accurate
 127 results in the most critical situations.

128 In order to explain the above-mentioned methods, the paper introduces at
 129 first the model used for describing the electro-mechanical system in Section 2.
 130 This also allows to present one of the methods currently used for estimating
 131 C_s , which will be employed in this paper as reference method in order to show
 132 the reliability and the effectiveness of the newly proposed techniques. Then,
 133 these proposed methods are described in Section 3, while Section 4 explains
 134 the new approach for estimating the modal electro-mechanical coupling factor.
 135 Finally, Section 5 discusses the experimental campaign carried out to validate
 136 the proposed techniques and show their results.

137 2. System model

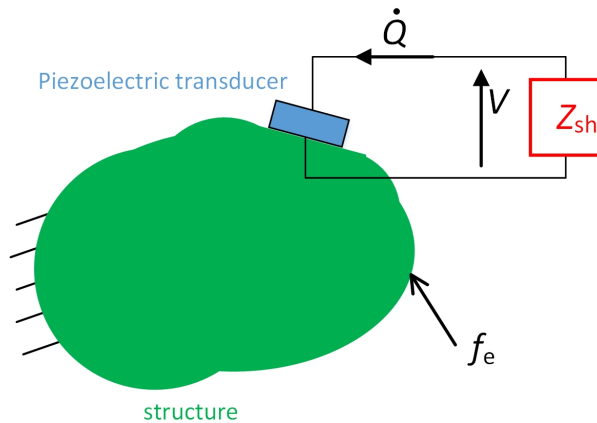


Figure 1: Piezoelectric shunt by means of an impedance Z_{sh} .

138 The dynamics of a vibrating system with a bonded piezoelectric transducer
 139 and excited by an external force f_e (see Fig. 1) can be described, in modal
 140 coordinates, by the following equation [26, 41]:

$$(-\omega^2 + 2i\zeta_s\omega_s\omega + \omega_s^2)u_s - \theta_s V = f_{e,s} \quad \text{for } s = 1, \dots, N \quad (1)$$

141 where ω is the angular frequency, ω_s is the s -th eigenfrequency (with the piezo-
 142 electric transducer short-circuited), ζ_s is the associated non-dimensional damp-
 143 ing ratio, $f_{e,s}$ is the modal forcing, θ_s is a coupling coefficient per unit modal
 144 mass and V is the voltage across the electrodes of the piezoelectric transducer
 145 (see Fig. 1). Finally, i is the imaginary unit, u_s is the s -th modal coordinate
 146 and N is the number of modes (theoretically N is infinite).

147 The electric behaviour of the system is governed by the following expression
 148 [63]:

$$C_\infty V + \frac{V}{i\omega R_0} - Q + \sum_{s=1}^N \theta_s u_s = 0 \quad (2)$$

149 where Q is the charge in one of the electrodes of the piezoelectric transducer (see
 150 Fig. 1) and R_0 is the inherent resistance of the piezoelectric transducer (that is
 151 often neglected because it is very high). Moreover, \dot{Q} defines the current flowing
 152 in the circuit (i.e. the dot represents the derivative with respect to the time,
 153 see Fig. 1) and, as mentioned, C_∞ is the value of the piezoelectric capacitance
 154 at infinite frequency.

155 Assuming absence of external forcing (i.e. $f_e=0$ and thus $f_{e,s}=0$), Eq. (1)
 156 allows to derive the expression of the modal coordinate u_s as a function of the
 157 voltage V at the piezoelectric terminals:

$$u_s = \frac{\theta_s}{-\omega^2 + 2i\zeta_s\omega_s\omega + \omega_s^2} V \quad \text{for } s = 1, \dots, N \quad (3)$$

158 Substituting Eq. (3) into Eq. (2), the expression of the admittance $Y(i\omega)$ of the
 159 piezoelectric transducer attached to the structure can be obtained, evidencing
 160 the contribution of the dynamics of the mechanical system:

$$Y = \frac{\dot{Q}}{V} = \frac{i\omega Q}{V} = i\omega \left(C_\infty + \frac{1}{i\omega R_0} + \sum_{s=1}^N \frac{\theta_s^2}{-\omega^2 + 2i\zeta_s\omega_s\omega + \omega_s^2} \right) \quad (4)$$

161 If only the s -th mode is taken into account, thus considering a single-degree-
 162 of-freedom (SDOF) approximation, the modal sum in Eq (4) can be expressed
 163 as the sum of three terms: one due to the considered mode and other two
 164 accounting for the residual contributions of the neglected modes (i.e. higher
 165 and lower). Therefore, in the frequency range around ω_s (i.e. for $\omega \simeq \omega_s$), it
 166 is possible to approximate the capacitance of the piezoelectric transducer as a
 167 function of the frequency, $C(\omega)$, with the following expression:

$$C = \frac{B}{\omega} = \frac{\text{Im}\{Y\}}{\omega} = \text{Im}\left\{i\left(C_\infty + \frac{1}{i\omega R_0} + \frac{1}{-\omega^2 L'_s} + \frac{\theta_s^2}{-\omega^2 + 2i\zeta_s \omega_s \omega + \omega_s^2} + C'_s\right)\right\} \quad (5)$$

168 where $\text{Im}\{\}$ indicates the imaginary part of a complex quantity, $B(\omega) = \text{Im}\{Y(i\omega)\}$
 169 is the susceptance of the piezoelectric transducer attached to the structure and
 170 L'_s and C'_s are constants accounting for the contribution of the modes lower and
 171 higher than the s -th, respectively:

$$\sum_{n=1}^{s-1} \frac{\theta_n^2}{-\omega^2 + 2i\zeta_n \omega_n \omega + \omega_n^2} \simeq \sum_{n=1}^{s-1} \frac{\theta_n^2}{-\omega^2} = \frac{1}{-\omega^2 L'_s} \quad (6)$$

$$\sum_{n=s+1}^N \frac{\theta_n^2}{-\omega^2 + 2i\zeta_n \omega_n \omega + \omega_n^2} \simeq \sum_{n=s+1}^N \frac{\theta_n^2}{\omega_n^2} = C'_s \quad (7)$$

172 The letters used to indicate the contributions from the out-of-band modes are
 173 related to the equivalent effect of the two terms on the admittance of the piezo-
 174 electric transducer attached to the structure (see Eq. (4)). Indeed, C'_s has the
 175 units of a capacitance and translates into an additional contribution to C_∞ ,
 176 while L'_s has the units of an inductance and, thus, shows that the modes lower
 177 than the s -th provide an inductive contribution to the behaviour of the electrical
 178 part of the whole system around ω_s . It follows that the piezoelectric capacitance
 179 $C(\omega)$ can be expressed as:

$$C = C_s + \frac{1}{-\omega^2 L'_s} + \operatorname{Re}\left\{\frac{\theta_s^2}{-\omega^2 + 2i\zeta_s \omega_s \omega + \omega_s^2}\right\} = \quad (8)$$

$$C_s + \frac{1}{-\omega^2 L'_s} + \frac{\theta_s^2(-\omega^2 + \omega_s^2)}{(-\omega^2 + \omega_s^2)^2 + (2\zeta_s \omega_s \omega)^2}$$

180 where $\operatorname{Re}\{\}$ indicates the real part of a complex quantity.

The term C_s in Eq. (8) represents the modal capacitance and is the sum of C_∞ and C'_s . In order to estimate C_s , the admittance $Y(i\omega)$ of the piezoelectric transducer attached to the structure can be measured as a function of ω by means of an impedance analyzer. Then, the experimental curve describing $C(\omega)$ can be obtained from the admittance $Y(i\omega)$ or the susceptance as:

$$C(\omega) = \frac{B}{\omega} = \frac{\operatorname{Im}\{Y\}}{\omega} \quad (9)$$

181 It is then possible to estimate the unknowns C_s and L'_s by fitting the model in
 182 Eq. (8) to the experimental curve of $C(\omega)$ obtained by measuring $Y(i\omega)$ and
 183 employing Eq. (9). The values of ω_s and ζ_s are considered known in Eq. (8)
 184 because they can be estimated by modal analysis. Considering θ_s^2 in Eq. (8),
 185 in case of low modal superimposition, it can be expressed as a function of the
 186 modal electro-mechanical coupling factor k_s . Indeed, the relation between k_s
 187 and θ_s is [60]:

$$\theta_s^2 = k_s^2 \omega_s^2 C_s \quad (10)$$

188 The modal electro-mechanical coupling factor k_s can be approximated by es-
 189 timating the short- (i.e. ω_s) and open-circuit (i.e. $\hat{\omega}_s$) eigenfrequencies of the
 190 system as:

$$k_s^2 = \frac{\hat{\omega}_s^2 - \omega_s^2}{\omega_s^2} \quad (11)$$

191 Therefore, θ_s^2 can be approximated as (combine Eqs. (11) and (10)):

$$\theta_s^2 = C_s (\hat{\omega}_s^2 - \omega_s^2) \quad (12)$$

192 Equation (12) shows that θ_s^2 can be approximated as the product of the known
 193 quantity $(\hat{\omega}_s^2 - \omega_s^2)$ (indeed, also $\hat{\omega}_s$ can be estimated by means of a modal
 194 analysis of the system) and C_s which is, together with L'_s , the unknown in
 195 Eq. (8). However, θ_s^2 can also be considered as an unknown and found by
 196 means of the minimisation, together with C_s and L'_s , in order to improve the
 197 fit, correcting a possible non-accurate initial estimation of θ_s^2 .

198 This procedure employed to estimate the value of C_s and based on the use
 199 of an impedance analyzer will be the reference method in this paper. Therefore,
 200 the two new methods for estimating the value of the modal capacitance C_s ,
 201 discussed in Section 3, will then be compared to this reference procedure (in
 202 Section 5).

203 3. Indirect methods for estimating the modal capacitance

204 The two methods presented here require to connect a shunt impedance Z_{sh}
 205 to the piezoelectric transducer (see Fig. 1). The possibility to identify system
 206 parameters by connecting a known impedance to the piezoelectric transducer
 207 was sketched in [39]. Here, this approach is applied to the modal capacitance
 208 and is developed and investigated. The first method requires that Z_{sh} is an
 209 inductance L (see Section 3.1), while Z_{sh} is a negative capacitance (NC) $-C_n$
 210 for the second method (see Section 3.2).

211 3.1. Method 1: L -based estimation of the modal capacitance

212 When an inductance is shunted to the piezoelectric transducer (i.e. $Z_{sh} =$
 213 $i\omega L$), the relation between the charge and the voltage at the piezoelectric ter-
 214 minals can be expressed as:

$$Q = \frac{V}{L\omega^2} \quad (13)$$

215 By using Eq. (13) in the equations describing the electric behaviour of the
 216 system (see Eqs. (2), (6) and (7)), exploiting the SDOF approximation and
 217 neglecting R_0 , the following equality is obtained:

$$V = \frac{-\theta_s L \omega^2}{C_s L \omega^2 - 1} u_s \quad (14)$$

218 To obtain this equation, the term related to L'_s has been neglected. Indeed,
 219 according to the literature (e.g. [60, 65]), $1/L'_s$ is low enough to be neglected in
 220 case of low modal superimposition.

221 When substituting Eq. (14) into Eq. (1) and only considering mode s to
 222 describe the dynamics of the system in the frequency range around ω_s because of
 223 the low modal superimposition hypothesis, the FRF displacement/force relation
 224 of the electro-mechanical system can be derived (assuming $\zeta_s \simeq 0$):

$$\frac{u_s}{f_{e,s}} = \frac{C_s L \omega^2 - 1}{(-\omega^2 + \omega_s^2)(C_s L \omega^2 - 1) + \theta_s^2 L \omega^2} \quad (15)$$

225 As expected, since a shunt impedance composed by an inductance L is used,
 226 the FRF in Eq. (15) governs four poles and, thus, the presence of the shunt
 227 impedance produces two peaks around ω_s , at $\omega_{s,1}$ and $\omega_{s,2}$, in the FRF dis-
 228 placement/force of the system (e.g. [62, 67]). These two eigenfrequencies can
 229 be found posing the denominator of the FRF in Eq. (15) equal to zero:

$$\omega^4 C_s L - \omega^2 [L(\theta_s^2 + C_s \omega_s^2) + 1] + \omega_s^2 = 0 \quad (16)$$

230 Solving Eq. (16), the analytical expressions of $\omega_{s,1}$ and $\omega_{s,2}$ can be found and
 231 the following equality can be obtained:

$$\omega_{s,1}^2 \omega_{s,2}^2 = \frac{\omega_s^2}{C_s L} \quad (17)$$

232 If $\omega_{s,1}$ and $\omega_{s,2}$ are estimated experimentally, Eq. (17) can be used to find
 233 C_s . The use of Eq. (17) is advantageous compared to the use of a single
 234 solution of Eq. (16) (i.e. either $\omega_{s,1}$ or $\omega_{s,2}$) because it allows to estimate C_s
 235 without estimating θ_s , and thus with a consequent decrease in the uncertainty
 236 associated to the estimate of C_s . **It is also noticed that the basic idea of Eq.**
 237 **(17) is to identify some features of a primary structure by observing how the**
 238 **coupling to a known system changes its dynamic behaviour. This is an approach**

239 successfully adopted in other applications and with different targets (e.g. modal
240 mass estimation [68]).

241 To summarise, the following steps are necessary to estimate C_s with the
242 L -based method:

- 243 • Measure the system FRF with the piezoelectric transducer terminals short-
244 circuited and estimate ω_s with an experimental modal analysis.
- 245 • Build an inductance L and measure/estimate its value. In theory, it could
246 have any value. However, it is good practice to choose a value that allows
247 to have two clear peaks for the shunted system FRF $u_s/f_{e,s}$. Such a
248 behaviour is obtained when the inductance is tuned on the considered
249 mode [26] and, thus, when its value is approximately:

$$L = \frac{1}{C_s \omega_s^2} \quad (18)$$

250 This would require to have a rough estimation of C_s in advance. However,
251 since a fine tuning is not necessary for the procedure (i.e. just the presence
252 of two clear peaks in the FRF is required), the first trial for the inductance
253 value can be obtained by using Eq. (18) with the capacitance C_{piezo} of
254 the piezoelectric patch commonly reported on the data-sheet from the
255 manufacturer.

- 256 • Connect the inductance to the piezoelectric transducer.
- 257 • Evaluate the system FRF $u_s/f_{e,s}$ around ω_s . If the experimental FRF
258 does not show two clear peaks around ω_s , the value of L can be changed
259 with a trial and error procedure until they are evident. It is important
260 to measure/estimate the final value of L used before performing the next
261 point on the list.
- 262 • Estimate $\omega_{s,1}$ and $\omega_{s,2}$ by experimental modal analysis on the measured
263 FRF.
- 264 • Use Eq. (17) to find C_s .

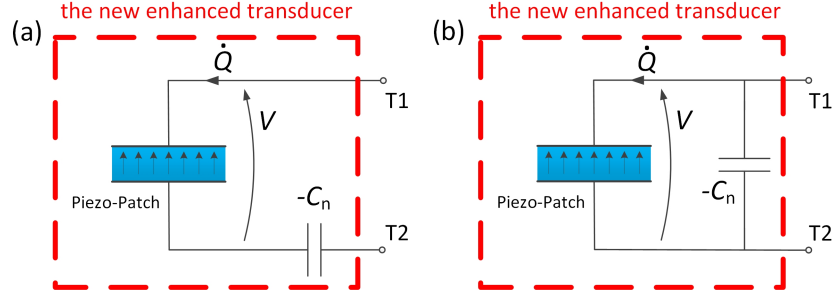


Figure 2: A piezoelectric transducer connected to an NC in series (a) and in parallel (b). The red dashed line indicates the new enhanced transducer composed by the piezoelectric transducer and the NC.

266 A shunt impedance composed by an NC, $-C_n$, is used in this case. The
 267 use of an NC allows to define a new enhanced transducer composed by the
 268 piezoelectric transducer and the NC, as evidenced in Fig. 2. The figure also
 269 shows that there are two possible connection layouts: series (see Fig. 2a) and
 270 parallel (see Fig. 2b). The capability of the NC to shift either the short- or
 271 open-circuit eigenfrequencies of the system is exploited here to estimate the
 272 modal capacitance.

273 Consider an electro-mechanical system with short-circuit eigenfrequencies
 274 equal to ω_s and open-circuit eigenfrequencies equal to [60] (see also Eqs. (11)
 275 and (10)):

$$\hat{\omega}_s = \sqrt{\omega_s^2 + \frac{\theta_s^2}{C_s}} \quad (19)$$

276 When an NC connected in series is used (see Fig. 2a), it shifts the short-
 277 circuit eigenfrequencies (i.e. short-circuiting the terminals T1 and T2 of the new
 278 enhanced transducer in Fig. 2a) towards lower frequency values [60]. The new
 279 values of the short-circuit eigenfrequencies are denoted here as ω_s^{sc} . Conversely,
 280 NCs connected in parallel (see Fig. 2b) shift the open-circuit eigenfrequencies
 281 (i.e. with the terminals T1 and T2 of the new enhanced transducer in Fig. 2b
 282 open-circuited) towards higher frequency values [60]. The new values of the

283 open-circuit eigenfrequencies are denoted here as ω_s^{oc} . It is also noticed that the
 284 two types of connection (series/parallel) require different values of the NC, as
 285 explained below.

286 According to [60], for an NC in series, the value of C_n must be set higher
 287 than the value of the piezoelectric capacitance at the null frequency C_0 to assure
 288 system stability (thus, the following inequalities hold $C_n > C_0 > C_s$). In this
 289 case, for low modal superimposition, the value of ω_s^{sc} can be expressed as:

$$\omega_s^{\text{sc}} = \omega_s \sqrt{1 - \frac{\theta_s^2}{\omega_s^2(C_n - C_s)}} \quad (20)$$

290 If the value of the NC used is known, as well as the short- and open-circuit
 291 eigenfrequencies (i.e. ω_s , $\hat{\omega}_s$ and ω_s^{sc}), it is possible to estimate the modal
 292 capacitance C_s combining Eqs. (20) and (19), without the need of estimating
 293 θ_s :

$$C_s = \frac{\omega_s^2 - (\omega_s^{\text{sc}})^2}{\hat{\omega}_s^2 - (\omega_s^{\text{sc}})^2} C_n \quad (21)$$

294 For an NC in parallel, the value of C_n must be set lower than C_∞ to assure
 295 system stability (thus, the following inequalities hold $C_n < C_\infty < C_s$), and the
 296 value of ω_s^{oc} is described by the following relation [60]:

$$\omega_s^{\text{oc}} = \omega_s \sqrt{1 + \frac{\theta_s^2}{\omega_s^2(C_s - C_n)}} \quad (22)$$

297 The estimate of C_s in this case can be obtained by combining Eqs. (22) and
 298 (19):

$$C_s = \frac{(\omega_s^{\text{oc}})^2 - \omega_s^2}{(\omega_s^{\text{oc}})^2 - \hat{\omega}_s^2} C_n \quad (23)$$

299 Therefore, the following procedure can be employed in order to estimate C_s :

- 300 • Measure the system FRF with the piezoelectric terminals short- and open-
- 301 circuited and estimate ω_s and $\hat{\omega}_s$, respectively, with an experimental modal
- 302 analysis.

- 303 • Build an NC $-C_n$ and measure/estimate its value. The NC must assure
 304 the stability of the system and, thus, a rough estimation of either C_0 or
 305 C_∞ is needed in advance. Such an estimation can be obtained by using the
 306 capacitance of the piezoelectric patch reported on the data-sheet of the
 307 manufacturer, C_{piezo} . Then, in case the system is unstable connecting the
 308 NC to the piezoelectric transducer, the value of the NC must be adjusted
 309 until stability is reached. It is important to measure/estimate the final
 310 value of C_n used before performing the next point on the list.
- 311 • Connect the NC to the piezoelectric transducer and evaluate the system
 312 FRF.
- 313 • Estimate either ω_s^{sc} or ω_s^{oc} , according to the type of connection of the NC
 314 used, by experimental modal analysis.
- 315 • Use either Eq. (21) or Eq. (23) to find C_s .

316 An advantage of this procedure is that it allows to estimate C_s for different
 317 modes at the same time, with a single value of the NC (i.e. the NC affects all
 318 the modes of the electro-mechanical system), while the L -based method allows
 319 to estimate C_s only for the mode on which L is tuned on.

320 The two methods for estimating the value of C_s described in this subsection
 321 and in Section 3.1 will be compared to the traditional fitting procedure (see
 322 Section 2) in Section 5. The next section shows how it is possible to estimate
 323 also θ_s and k_s from the L -based method used for estimating C_s .

324 4. Indirect methods for estimating the coupling coefficients

325 When the value of θ_s needs to be estimated, usually, Eq. (12) is used (which
 326 requires to have estimated C_s in advance) or θ_s is added among the unknowns
 327 in the fitting procedure described in Section 2. However, when a double check
 328 on the estimated θ_s value is recommended, the two methods presented in Sec-
 329 tions 3.1 and 3.2 to estimate C_s can be employed since they provide different

330 approaches for estimating θ_s , as explained in Section 4.1. Furthermore, the L -
 331 based method (Section 3.1) also allows for a further estimation of k_s (which is
 332 usually estimated with Eq. (11)). This additional method allows to decrease
 333 the uncertainty associated to the traditional estimation as shown in Section 4.2.

334 4.1. Indirect methods for estimating θ_s

335 When the piezoelectric transducer is shunted with an inductance L (see
 336 Section 3.1), the following relation between $\omega_{s,1}$ and $\omega_{s,2}$ can be derived from
 337 Eq. (16):

$$\omega_{s,1}^2 + \omega_{s,2}^2 = \omega_s^2 + \frac{\theta_s^2}{C_s} + \frac{1}{C_s L} \quad (24)$$

338 If the L -based method is used to estimate C_s , the only unknown in Eq. (24) is θ_s
 339 that can be, then, easily estimated. This θ_s estimate can be used, if needed, to
 340 check and verify the value coming from different estimation techniques. Indeed,
 341 it is noticed that the estimate of θ_s through Eq. (24) relies on the knowledge of
 342 parameters different from those on which Eq. (12) (or the fitting procedure) is
 343 based. Therefore, the procedures lead to different estimates of θ_s that can be,
 344 thus, compared.

345 Considering the NC-based method, the value of θ_s can be estimated using
 346 the expression of either ω_s^{sc} (Eq. (20)) or ω_s^{oc} (Eq. (22)), depending on the
 347 NC layout employed. Indeed, if C_s is estimated with the method described in
 348 Section 3.2, θ_s is the only unknown in Eqs. (20) and (22). Also in this case,
 349 the estimate of θ_s is obtained using parameters and expressions different from
 350 those traditionally employed (e.g. Eq. (12)). Therefore, the obtained θ_s values
 351 can be compared.

352 4.2. Indirect method for estimating k_s

353 This subsection shows a new method to estimate k_s relying on the connection
 354 between the piezoelectric transducer and an inductance L . Indeed, by substitu-
 355 tion of Eqs. (17) and (10) into Eq. (24), the modal electro-mechanical coupling
 356 factor can be expressed as a function of $\omega_{s,1}$, $\omega_{s,2}$ and ω_s [67]:

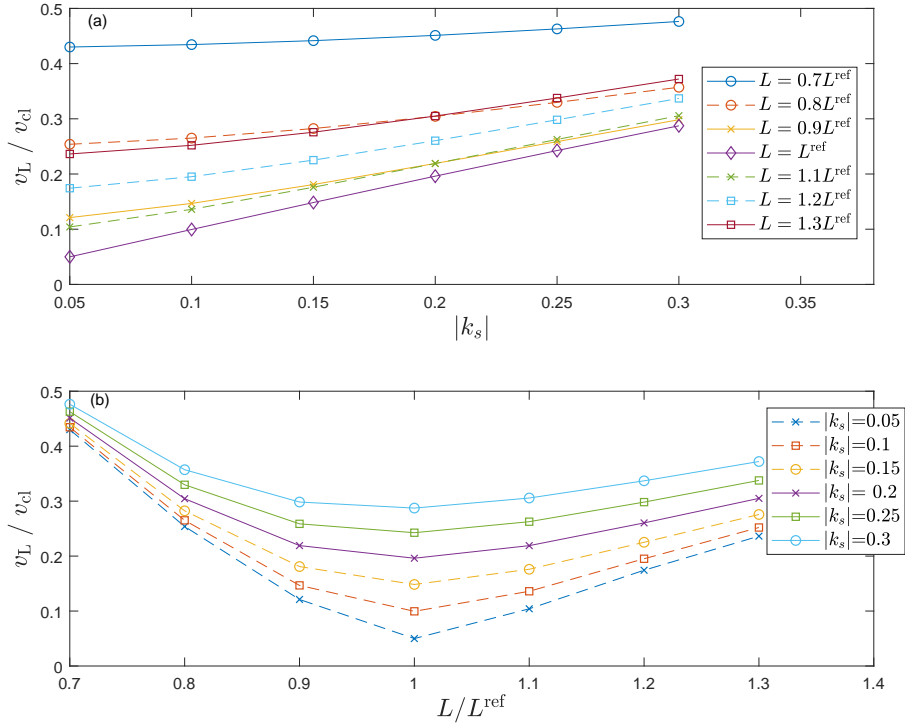


Figure 3: The trend of v_L/v_{cl} as a function of the $|k_s|$ value for different L values (a) and as a function of the ratio L/L^{ref} for different $|k_s|$ values. Here, $\zeta_s = 5 \times 10^{-4}$ and $C_s = 39$ nF (this value was chosen in order to stay close to the C_s values of the system used for the experiments in Section 5).

$$k_s^2 = \frac{\omega_{s,1}^2 + \omega_{s,2}^2}{\omega_s^2} - \frac{\omega_{s,1}^2 \omega_{s,2}^2}{\omega_s^4} - 1 \quad (25)$$

357 This formulation reduces to $k_s^2 = [(\omega_{s,1}^2 + \omega_{s,2}^2)/\omega_s^2] - 2$ in case $L = L^{\text{ref}}$, where
 358 L^{ref} denotes the value of the inductance in Eq. (18) (see Eqs. (17) and (18)). A
 359 first advantage of the formulation of Eq. (25) is that the estimate of k_s depends
 360 on ω_s and on the eigenfrequencies generated by the inductive shunt. Indeed,
 361 $\omega_{s,1}$ and $\omega_{s,2}$ are well separated and their distance is greater than that between
 362 ω_s and $\hat{\omega}_s$ on which the traditional estimation of k_s is based (see Eq. (11)).
 363 Therefore, in the case short- and open-circuit eigenfrequencies are really close
 364 each other and difficult to be identified with a good accuracy (e.g. low coupling

365 factor, low frequency), this new method allows to overcome the problem since it
 366 is based on the identification of eigenfrequencies more distant from each other.

367 Another advantage is related to the uncertainty associated to the coupling
 368 factor estimate. Indeed, estimating k_s with Eq. (25) provides a result with a
 369 reduced uncertainty compared to the case of using Eq. (11).

370 The standard uncertainty v of k_s^2 can be described by means of the com-
 371 bined uncertainty formulation [69], which is based on a Taylor expansion. This
 372 formulation requires an estimation of the uncertainty related to the estimation
 373 of the eigenfrequencies involved in the definition of k_s^2 (either Eq. (25) or Eq.
 374 (11)). Here, the estimations of the input quantities ω_s , $\hat{\omega}_s$, $\omega_{s,1}$ and $\omega_{s,2}$ are
 375 assumed as independent and the standard uncertainty associated to the estimates
 376 (evaluated by means of modal analysis) is assumed equal and here referred to
 377 as r . Assuming that the Taylor expansion can be truncated to the first order
 378 terms for the sake of simplicity, v assumes the following expression when k_s^2 is
 379 estimated with Eq. (11):

$$v = \sqrt{\left(\frac{\partial k_s^2}{\partial \omega_s} r\right)^2 + \left(\frac{\partial k_s^2}{\partial \hat{\omega}_s} r\right)^2} = 2r \frac{\hat{\omega}_s}{\omega_s^2} \sqrt{1 + \frac{\hat{\omega}_s^2}{\omega_s^2}} \quad (26)$$

380 Conversely, when k_s^2 is estimated with Eq. (25), v is:

$$v = \sqrt{\left(\frac{\partial k_s^2}{\partial \omega_s} r\right)^2 + \left(\frac{\partial k_s^2}{\partial \omega_{s,1}} r\right)^2 + \left(\frac{\partial k_s^2}{\partial \omega_{s,2}} r\right)^2} =$$

$$2r \frac{1}{\omega_s^5} \sqrt{4\omega_{s,1}^4 \omega_{s,2}^4 + \omega_s^2 (\omega_{s,1}^2 + \omega_{s,2}^2) (\omega_s^4 - 3\omega_{s,1}^2 \omega_{s,2}^2) + \omega_s^4 (\omega_{s,1}^2 - \omega_{s,2}^2)^2} \quad (27)$$

381 From here on, v is denoted as v_{cl} for the classical estimation method (see
 382 Eq. 26) and as v_L for the newly proposed method (see Eq. 27). The two
 383 uncertainties can be compared by calculating the ratio v_L/v_{cl} as a function of
 384 two parameters: k_s , which governs the distance between ω_s and $\hat{\omega}_s$, and L which
 385 affects the distance between $\omega_{s,1}$ and $\omega_{s,2}$. This analysis is shown in Fig. 3a
 386 where the different curves are related to different L values. The values of L are
 387 expressed as referenced to the L value of Eq. (18), denoted as L^{ref} in the figure.
 388 Looking at Fig. 3a, it can be seen that the influence of the L value is to modify

Table 1: Values of the components of the circuits in Fig. 5.

R_A	R_B	R_C	C_L	R_{p2}	R_1	R_2	\hat{R}	R_{comp}	\hat{C}
[k Ω]	[k Ω]	[k Ω]	[μ F]			[k Ω]		[M Ω]	[nF]
1.98	0.99	0.99	4.84	variable	variable	11.47	variable	2.91	69.23

389 the value of v_L because of the change of the values and relative distances of the
390 eigenfrequencies $\omega_{s,1}$ and $\omega_{s,2}$. However, regardless the value of the inductance
391 used, and despite that the ratio v_L/v_{cl} increases with k_s , it is evident that v_L is
392 always significantly lower than v_{cl} .

393 In order to clarify the influence of the value of L on v_L , it is noticed that
394 this relationship is not straightforward to be analysed because v_L depends on
395 both the distance between $\omega_{s,1}$ and $\omega_{s,2}$ and on their absolute values (see Eq.
396 (27)). Therefore, when L is changed, there are two effects to be considered and
397 they can have an opposite influence on the resulting value of v_L . However, Fig.
398 3b allows to achieve a clear conclusion about which L value is the one allowing
399 to reduce v_L as much as possible. In this figure, the trend of v_L/v_{cl} is depicted
400 as a function of the ratio L/L^{ref} for systems with different $|k_s|$ values. In all the
401 cases, the value of L equal to L^{ref} is always able to reduce as much as possible
402 v_L .

403 The next section describes the experimental tests carried out to validate the
404 methods presented in this subsection and in Section 3.

405 5. Experimental validation of the methods

406 This section presents the tests carried out to validate the L -based and NC-
407 based methods for estimating the modal capacitance and also the method pre-
408 sented in Section 4.2 for the estimation of $|k_s|$. At first, the set-up is described
409 in Section 5.1 and then the results of the tests are presented in Section 5.2.

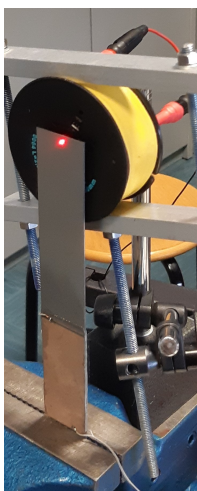


Figure 4: The set-up.

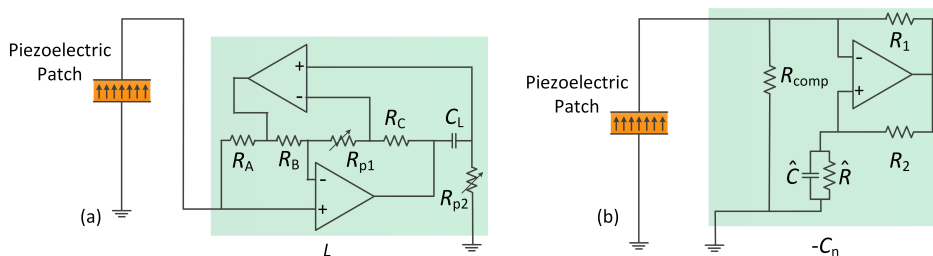


Figure 5: The electrical schematics used to build the shunt inductance for the L -based method (a) and the NC shunt for the NC-based method (b).

410 *5.1. The experimental set-up*

411 The set-up used was a stainless steel cantilever beam (length of about 18 cm,
 412 width of approximately 3 cm and thickness of about 1 mm) with two piezoelec-
 413 tric patches (length 70 mm, width 30.0 mm, thickness 0.55 mm, material PIC
 414 151) bonded at the clamped end (one per side) and electrically connected in se-
 415 ries (see Fig 4). The beam was forced by using a contactless actuator composed
 416 of a coil and a magnet bonded close to the tip (the force exerted to the beam was
 417 assumed as proportional to the measured current flowing through the coil [70]),
 418 while the structural response was measured by means of a laser velocimeter. The

419 measured FRFs velocity/force allowed to find the FRFs displacement/force just
420 by dividing them with $i\omega$.

421 Considering the L -based method for the estimation of C_s and $|k_s|$, the tests
422 were carried out on the first bending mode of the beam. The main reason
423 for choosing the first mode of the beam was to have an eigenfrequency with
424 a low value (approximately 32 Hz) and thus a high value for L (e.g. see Eq.
425 (18)). In this way, it was possible to demonstrate the practical feasibility of the
426 L -based method also in a disadvantageous situation. Indeed, since the value
427 required for L was high, a synthetic inductor was built by using the Antoniou's
428 circuit [26, 71] based on operational amplifiers. The circuit is shown in Fig.
429 5a. Here, the variable resistance R_{p1} was used in order to produce a negative
430 resistance in series with L . This negative resistance was needed to eliminate
431 parasitic resistances that can be present when using operational amplifiers to
432 simulate inductances. The total residual resistance was estimated to 500 Ω ,
433 that was considered a value low enough not to affect the experimental tests
434 (also according to simulations).

435 For the NC-based method, the NC was connected in series in order to work
436 on the first bending modes of the beam [60]. The circuit used was that of
437 Fig. 5b. It can be modelled as the parallel connection of an NC and a negative
438 resistance. The value of R_{comp} was chosen in order to make the resistance highly
439 negative (i.e. -75 M Ω). This allows the circuit of Fig. 5b to behave like a pure
440 NC. More details about this circuit can be found in [60].

441 The values used for the components of the circuits of Fig. 5 are provided
442 in Table 1. All the operational amplifiers used were of type OPA445 and were
443 supplied with a voltage of ± 30 V.

444 Considering the tests with the reference method for estimating C_s described
445 in Section 2 (i.e. the fitting procedure), they were performed with an impedance
446 analyzer.

447 Finally, the modal parameters (e.g. eigenfrequencies) which are needed for
448 using the methods proposed in this paper were identified via modal analysis by
449 means of a least-squares complex-frequency domain method (e.g. [72]).

Table 2: Values of ω_s , ζ_s and $\hat{\omega}_s$ for one of the tests.

bending mode	$\omega_s/(2\pi)$ [Hz]	ζ_s	$\hat{\omega}_s/(2\pi)$ [Hz]
1	32.48	4.2×10^{-3}	33.40
2	154.09	7.2×10^{-3}	154.53
3	437.67	1.7×10^{-3}	440.05

Table 3: Values of L and C_n used in the tests.

	test 1	test 2	test 3	test 4	test 5	test 6	test 7
L [H]	$607.9 \simeq L^{\text{ref}}$	589.7	571.4	553.2	534.9	516.7	-
C_n [nF]	112.9	87.8	79.0	71.9	65.9	60.8	56.5

450 5.2. Tests

451 At first, the tests related to the estimation of C_s are discussed here. These
452 tests lasted an entire day. The measurement with the impedance analyzer was
453 repeated three times during the day (before the tests with the L -based method,
454 between the tests with L -based and NC-based methods, and after all tests had
455 been conducted). Therefore, the effect of the temperature change, that inher-
456 ently occurred during the day in the lab, on the value of the modal capacitance
457 is present in the results of the reference method. This was unavoidable because
458 the tests for both the L -based and NC-based methods lasted some hours and
459 could not be performed at the same nominal temperature (the temperature in
460 the room of the tests can change of few degrees during the day). Together with
461 the tests using the impedance analyzer, also tests forcing the structure were
462 performed continuously in order to estimate each time the values of ω_s , ζ_s and
463 $\hat{\omega}_s$. Their values for one of these tests are reported in Table 2.

464 The tests with the L -based approach were carried out with six different
465 values of L (gathered in Table 3). This allowed to check the dispersion of the
466 results of the method. Seven tests were carried out for the NC-based method,
467 with seven different values of the NC (see Table 3). Since the aim of the new
468 proposed methods is to have an inexpensive approach for estimating C_s , the
469 values of L and C_n were not measured (this would require a device able to

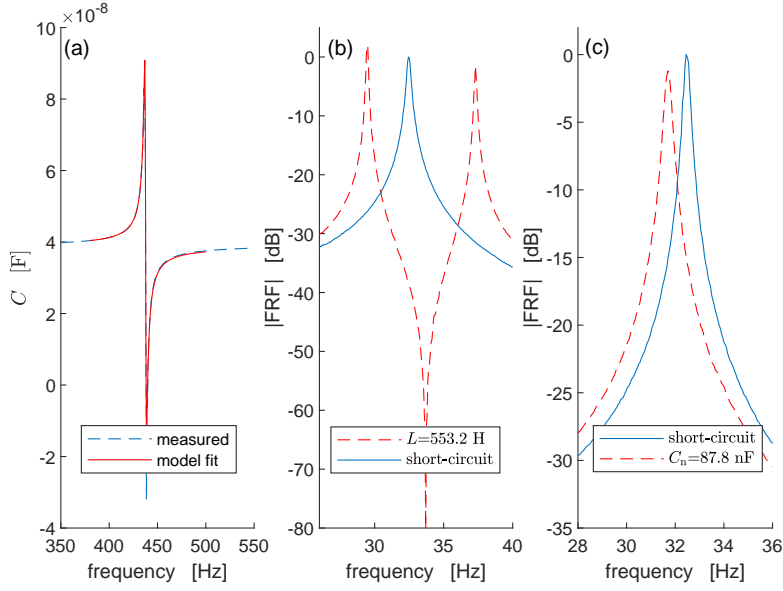


Figure 6: Fit of the capacitance of the piezoelectric patch at the third mode for one of the tests with the impedance analyzer (a), magnitude of the measured FRFs of the system (displacement/force) at the first mode showing the effect of the addition of L in method 1 (b), and magnitude of the measured FRFs of the system (displacement/force) at the first mode showing the shift of the short-circuit eigenfrequency due to the NC in method 2 (c).

470 characterise an active element), but theoretical formulas were instead employed
 471 directly to estimate the L and C_n values. This allows to test both the methods
 472 without the use of any additional device. More precisely, L was estimated as
 473 (refer to the elements in Fig. 5a):

$$L = \frac{C_L R_A R_C R_{p2}}{R_B} \quad (28)$$

474 and C_n was estimated as (refer to the elements in Fig. 5b):

$$C_n = \frac{R_2}{R_1} \hat{C} \quad (29)$$

475 The resistances and capacitances in Eqs. (28) and (29) were measured with an
 476 inexpensive basic multimeter.

477 Figures 6a, b and c show the fit of the capacitance of the piezoelectric

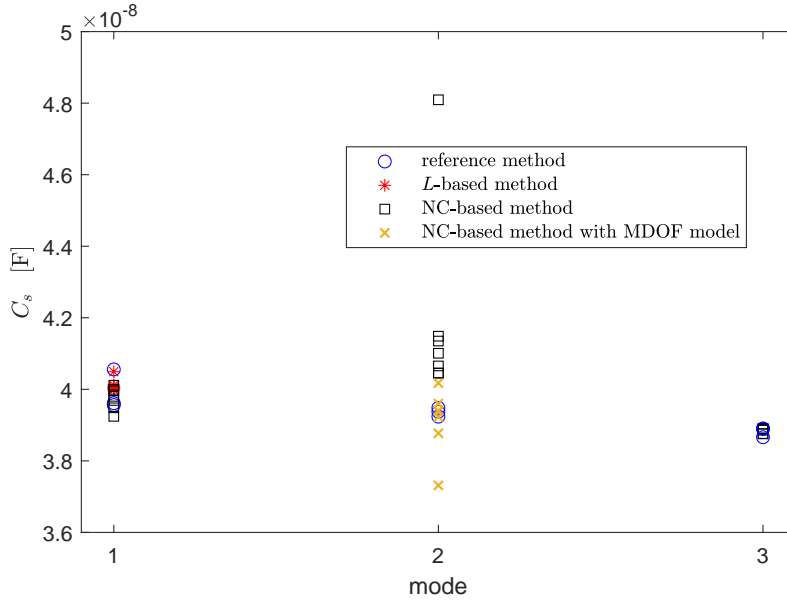


Figure 7: Results of the L -based and NC-based methods compared to the reference method for the first three modes of the beam.

478 patch with the model of Eq. (8) (setting C_s , L'_s and θ_s as the unknowns to
 479 be found) around the third bending mode of the beam for one of the tests with
 480 the impedance analyzer (a), the system FRF showing the influence of the addi-
 481 tional L in method 1 (b), and the system FRF with the shift of the short-circuit
 482 eigenfrequency due to the NC in series in method 2 (c), respectively.

483 Figure 7 shows the C_s results of the different methods for the first three
 484 bending modes of the beam (obviously, the results for the L -based method are
 485 absent for the second and third mode). There is a good superimposition among
 486 the different results for the first mode and the reproducibility of the different
 487 methods is comparable (see the magnification in Fig. 8a). In the case of the
 488 third mode, again, the results are more than satisfactory (see the magnification
 489 in Fig. 8b). Conversely, for the second mode, there is a bias between the results
 490 of the reference method and of the NC-based method (although, the order of
 491 magnitude of the results of the two methods is the same). The reason for this
 492 discrepancy is that the first mode peak is much higher than for the second

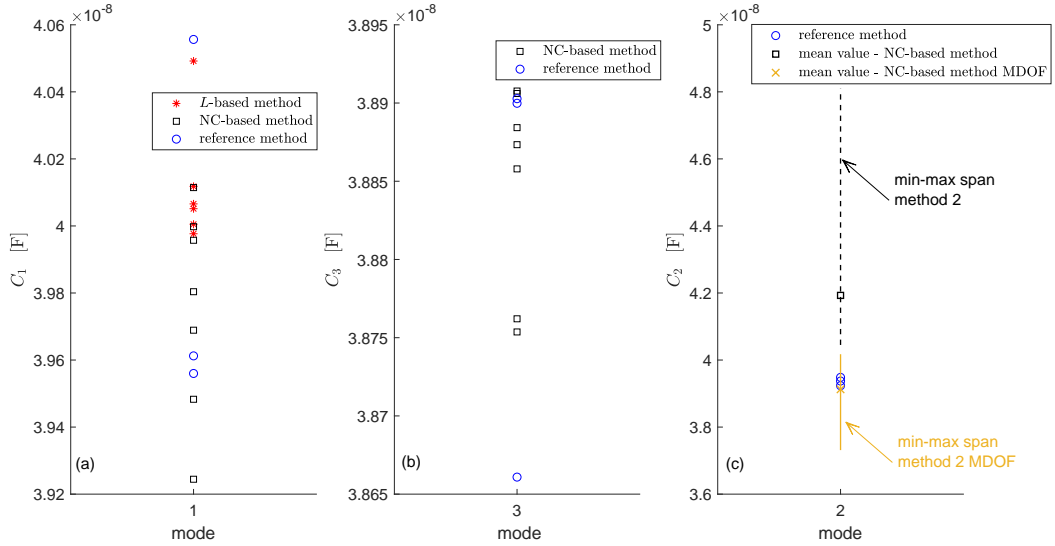


Figure 8: Results of different methods for the first (a), third (b) and second (c) bending mode.

493 mode in the displacement/force FRF of the system (due to higher eigenmode
 494 components). This makes the hypothesis of low modal coupling (which is at the
 495 foundation of the method) not valid for $\omega \simeq \omega_2$ with a non-negligible influence
 496 from the first mode. Therefore, to face situations like these, in which the modal
 497 superimposition is too large, a modified approach is needed. The solution is to
 498 adopt a multi-degree-of-freedom (MDOF) model to take into account the first
 499 two modes of the beam (those interesting for the problem) and the effect of the
 500 NC. Such a model, developed in [63], is briefly described in Appendix A, while
 501 in this section only the results are discussed (represented with yellow crosses
 502 in Fig. 7). The use of the MDOF model allows to improve the estimation of
 503 C_s , eliminating the previously evidenced bias. Finally, Fig. 8c shows, for the
 504 second mode, the results of the reference method superimposed to the mean
 505 value of the results of the NC-based method with the SDOF (black square)
 506 and MDOF (yellow cross) models. The solid lines show the spans between
 507 the largest and smallest results for the two types of NC-based method. This
 508 allows to stress the benefits provided in this case by the MDOF approach and
 509 to evidence the reliability of the proposed method even in case of significant

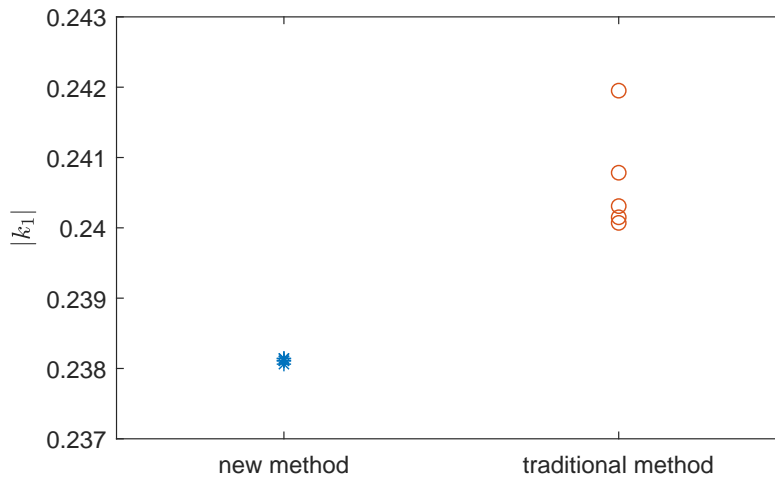


Figure 9: The estimation of $|k_1|$ with the classical experimental approach (see Eq. (11)) and the newly proposed one related to the connection of the piezoelectric patch to an inductance (see Eq. (25)).

510 modal superimposition. Obviously, in a real application, one should analyse
 511 the system FRF in order to evaluate whether the MDOF approach is needed or
 512 the SDOF one can be employed. It is also important to notice that the same
 513 MDOF approach can be used with the L -based method with similar results as
 514 those obtained for the NC-based method. **Therefore, even if the L -based and**
 515 **NC-based methods have been initially presented under the hypothesis of low**
 516 **modal superimposition, the results shown above enable to evidence that they**
 517 **can provide reliable estimations of C_s also when this hypothesis is not fulfilled,**
 518 **by using the MDOF model.**

519 As a concluding remark, it is possible to suggest to always carry out more
 520 than one measurement of C_s when using either the L -based or the NC-based
 521 method. Indeed, the mean value of the results is expected to be a reliable
 522 estimator of the modal capacitance.

523 Finally, the newly proposed method to estimate $|k_s|$ (see Section 4.2) was
 524 tested on the first bending mode of the beam. To this purpose, a modal analysis
 525 was repeated five times with the piezoelectric patch in both short- and open-
 526 circuit. This allowed to estimate five values of $|k_1|$ with Eq. (11). Furthermore,

527 also a modal analysis with the piezoelectric patch connected to an inductance
528 like that of test 2 in Table 3 was repeated five times, allowing to obtain five values
529 of $|k_1|$ estimated through Eq. (25). The results are shown in Fig. 9. A slight
530 bias (i.e. different mean values) can be evidenced between the results of the two
531 methods. This is mainly due to thermal changes during the test session of the
532 two methods. However, this bias is so small that it can be considered negligible
533 for practical applications. The interesting outcome of this figure is that the
534 result dispersion related to the new method is much lower compared to the
535 classical method, therefore implying a lower uncertainty. This is in accordance
536 with the uncertainty analysis performed in Section 4.2 (particularly, see Fig. 3).

537 6. Conclusion

538 This paper has described two indirect methods for estimating the value of the
539 modal capacitance for piezoelectric transducers using vibration measurements
540 and low-cost electronic devices, thus avoiding the measurement of electrical
541 voltage and current. This results in an inexpensive experimental set-up. One
542 method requires to connect the piezoelectric transducer to an inductance L ,
543 while the other to an NC. Furthermore, the L -based method also allows for
544 an estimation of the modal electro-mechanical coupling factor affected by less
545 uncertainty compared to what occurs for the usual experimental estimation
546 approach.

547 Considering the estimation of the modal capacitance, both methods have
548 been validated against one of the reference methods available in the literature,
549 showing satisfactory performances. Indeed, the results have been in accordance
550 with those provided by the reference method and also the result dispersion was
551 comparable. The paper has also shown that it is possible to successfully esti-
552 mate the modal capacitance even when the modal superimposition is significant.
553 This is possible by using an MDOF model for the NC-based method (a similar
554 approach is possible also for the L -based method).

555 Considering the estimation of the modal electro-mechanical coupling factor,

556 the experimental results proved the capability of the L -based method to pro-
557 vide estimations of $|k_s|$ with lower uncertainty than the classical experimental
558 method commonly used to estimate it.

559 Appendix A. The MDOF model

560 This appendix briefly recalls the basics of the MDOF model presented in [63].
561 The system with the open-circuited piezoelectric transducer is represented by
562 means of a state space model. The matrices of this model depend on the modal
563 parameters of the structure (i.e. eigenfrequencies and eigenvector components
564 scaled to the unit modal mass with the short-circuited piezoelectric transducer
565 and associated non-dimensional damping ratios for the first two bending modes
566 of the system, i.e. $s=1,2$) that can be estimated by means of modal analysis.
567 In this specific case, the matrices depend on three further variables:

- 568 1. θ_1 : it can be estimated finding C_1 with the NC-based method (see Section
569 3.2) and then inserting this C_1 value into Eq. (12). It is recalled that
570 C_1 can be directly estimated with the method of Section 3.2 because the
571 corresponding mode is not severely influenced by the surrounding modes.
- 572 2. C_2 : it is the unknown of the problem.
- 573 3. θ_2 : it can be expressed as a function of the unknown C_2 by using Eq. (12).

574 The expressions of the matrices are as follows:

$$\mathbf{A} = \begin{bmatrix} -2\omega_1\zeta_1 & -\omega_1^2[1 + \theta_1^2/(\omega_1^2 C_2)] & 0 & -(\theta_1\theta_2)/C_2 & -\theta_1/(R_0 C_2 \sqrt{C_2}) \\ 1 & 0 & 0 & 0 & 0 \\ 0 & -(\theta_1\theta_2)/C_2 & -2\omega_2\zeta_2 & -\omega_2^2[1 + \theta_2^2/(\omega_2^2 C_2)] & -\theta_2/(R_0 C_2 \sqrt{C_2}) \\ 0 & 0 & 1 & 0 & 0 \\ 0 & -\theta_1/\sqrt{C_2} & 0 & -\theta_2/\sqrt{C_2} & -1/(R_0 C_2) \end{bmatrix} \quad (\text{A.1})$$

$$\mathbf{B}_f^T = \begin{bmatrix} \phi_1(x_f) & 0 & \phi_2(x_f) & 0 & 0 \end{bmatrix} \quad (\text{A.2})$$

$$\mathbf{B}_w^T = \begin{bmatrix} \theta_1/\sqrt{C_2} & 0 & \theta_2/\sqrt{C_2} & 0 & 1 \end{bmatrix} \quad (\text{A.3})$$

$$\mathbf{C}_z = \begin{bmatrix} 0 & \phi_1(x_m) & 0 & \phi_2(x_m) & 0 \end{bmatrix} \quad (\text{A.4})$$

$$\mathbf{C}_y = \begin{bmatrix} 0 & 0 & 0 & 0 & -1 \end{bmatrix} \quad (\text{A.5})$$

575 in which $\phi_s(x_f)$ and $\phi_s(x_m)$ are the eigenvector components (scaled to the unit
 576 modal mass and with the piezoelectric transducer short-circuited) of mode s at
 577 locations x_f (i.e. where the disturbance f_e is applied) and x_m (i.e. where the
 578 system response is collected), respectively, with the superscript T indicating the
 579 matrix transpose.

580 These matrices form the following state space description of the electro-
 581 mechanical system:

$$\begin{cases} \dot{\mathbf{g}} = \mathbf{A}\mathbf{g} + \mathbf{B}_w\bar{Q} + \mathbf{B}_f f_e \\ w(x_m) = \mathbf{C}_z\mathbf{g} \\ y = \mathbf{C}_y\mathbf{g} \end{cases} \quad (\text{A.6})$$

582 where $w(x_m)$ is the displacement of the system in x_m , y is the output of the
 583 system, $\bar{Q} = Q/\sqrt{C_2}$ and \mathbf{g} is the vector containing the state variables:

$$\mathbf{g}^T = \begin{bmatrix} \dot{u}_1 & u_1 & \dot{u}_2 & u_2 & \int \bar{V} \end{bmatrix} \quad (\text{A.7})$$

584 where the symbol $\int \bar{V}$ is used to indicate the integral with respect to the time
 585 of \bar{V} , with $\bar{V} = V\sqrt{C_2}$.

586 The effect of the shunt impedance in this model is that of a controller which
 587 acts via a feedback loop. Therefore, in this case where the shunt impedance is
 588 an NC, the system results controlled by means of a controller which depends
 589 on the values of C_n and C_2 . The transfer function K_{nc} of the controller in the
 590 Laplace domain (the Laplace operator is defined here as S) is:

$$K_{nc} = \frac{\bar{Q}}{y}(S) = \frac{-C_n S}{C_2} \quad (\text{A.8})$$

591 Using the previously defined matrices and controller transfer function, the trans-
 592 fer function T_{wf} of the shunted system between f_e and $w(x_m)$ can be written
 593 as:

$$T_{wf}(S) = \mathbf{C}_z(\mathbf{S}\mathbf{I} - [\mathbf{A} + \mathbf{B}_w K_{nc} \mathbf{C}_y])^{-1} \mathbf{B}_f \quad (\text{A.9})$$

594 where \mathbf{I} is the identity matrix.

595 From this transfer function displacement/force, the corresponding FRF can
 596 be easily obtained. If this FRF with the shunted NC is experimentally measured,
 597 it can be used for fitting the model of the controlled system with C_2 as the only
 598 unknown to be tuned.

599 In case of doubt about the accuracy of the estimation of θ_1 because of closed
 600 modes (suppose to consider a system different from that tested), its initial value
 601 can be estimated by using the approach described in the first point in the
 602 previous numbered list and then it can be included in the model as a variable
 603 to be tuned through the minimisation, together with C_2 .

604 Finally, it is noticed that the tests used to estimate θ_1 (see the first point in
 605 the previous numbered list) are the same employed to find C_2 with the fitting
 606 procedure, using the MDOF model, and no repetition of the tests is therefore
 607 needed.

608 A similar MDOF model can be used also when employing an inductance L
 609 to shunt the piezoelectric transducer.

610 **Acknowledgment**

611 This research has financially been supported at University of Parma by the
 612 Programme "FIL-Quota Incentivante" of University of Parma and co-sponsored
 613 by Fondazione Cariparma. Furthermore, the Italian Ministry of Education,
 614 University and Research is acknowledged by S. Manzoni (Politecnico di Milano)
 615 for the support provided through the Project "Department of Excellence LIS4.0
 616 - Lightweight and Smart Structures for Industry 4.0".

617 **References**

- 618 [1] C. Fuller, S. Elliott, P. Nelson, Active control of vibration, Academic Press,
619 1997.
- 620 [2] A. Preumont, B. de Marneffe, A. Deraemaeker, F. Bossens, The damping of
621 a truss structure with a piezoelectric transducer, Computers and Structures
622 86 (3-5) (2008) 227–239. doi:10.1016/j.compstruc.2007.01.038.
- 623 [3] D. Meng, P. Xia, K. Lang, E. Smith, C. Rahn, Neural network based hys-
624 teresis compensation of piezoelectric stack actuator driven active control of
625 helicopter vibration, Sensors and Actuators, A: Physical 302 (2020) Article
626 Id 111809. doi:10.1016/j.sna.2019.111809.
- 627 [4] Q. Hu, G. Ma, Variable structure control and active vibration suppres-
628 sion of flexible spacecraft during attitude maneuver, Aerospace Science and
629 Technology 9 (4) (2005) 307–317. doi:10.1016/j.ast.2005.02.001.
- 630 [5] M. Sabatini, G. Palmerini, P. Gasbarri, Synergetic approach in atti-
631 tude control of very flexible satellites by means of thrusters and pzt de-
632 vices, Aerospace Science and Technology 96 (2020) Article ID 105541.
633 doi:10.1016/j.ast.2019.105541.
- 634 [6] G. Song, V. Sethi, H. N. Li, Vibration control of civil structures using
635 piezoceramic smart materials: A review, Engineering Structures 28 (11)
636 (2006) 1513–1524. doi:10.1016/j.engstruct.2006.02.002.
- 637 [7] P. Shivashankar, S. Gopalakrishnan, Review on the use of piezoelectric
638 materials for active vibration, noise, and flow control, Smart Materials and
639 Structures 29 (5) (2020) article ID: 053001. doi:10.1088/1361-665X/ab7541.
- 640 [8] Y. Luo, X. Zhang, Y. Zhang, Y. Qu, M. Xu, K. Fu, L. Ye, Active vibration
641 control of a hoop truss structure with piezoelectric bending actuators based
642 on a fuzzy logic algorithm, Smart Materials and Structures 27 (8) (2018)
643 Article ID 085030. doi:10.1088/1361-665X/aad1b6.

- 644 [9] S. Narayanan, V. Balamurugan, Finite element modelling of piezolami-
645 nated smart structures for active vibration control with distributed sensors
646 and actuators, *Journal of Sound and Vibration* 262 (3) (2003) 529–562.
647 doi:10.1016/S0022-460X(03)00110-X.
- 648 [10] S. Kang, H. Wu, X. Yang, Y. Li, Y. Wang, Fractional-order robust
649 model reference adaptive control of piezo-actuated active vibration iso-
650 lation systems using output feedback and multi-objective optimization
651 algorithm, *Journal of Vibration and Control* 26 (1-2) (2020) 19–35.
652 doi:10.1177/1077546319875260.
- 653 [11] C. M. Vasques, J. Dias Rodrigues, Active vibration control of smart
654 piezoelectric beams: Comparison of classical and optimal feedback con-
655 trol strategies, *Computers and Structures* 84 (22-23) (2006) 1402–1414.
656 doi:10.1016/j.compstruc.2006.01.026.
- 657 [12] J. Peng, G. Zhang, M. Xiang, H. Sun, X. Wang, X. Xie, Vibration control
658 for the nonlinear resonant response of a piezoelectric elastic beam via time-
659 delayed feedback, *Smart Materials and Structures* 28 (9) (2019) article ID:
660 095010. doi:10.1088/1361-665X/ab2e3d.
- 661 [13] J. Hu, Z. Kang, Topological design of piezoelectric actuator layer for lin-
662 ear quadratic regulator control of thin-shell structures under transient
663 excitation, *Smart Materials and Structures* 28 (9). doi:10.1088/1361-
664 665X/ab1e96.
- 665 [14] M. Moretti, E. Silva, J. Reddy, Topology optimization of flextensional
666 piezoelectric actuators with active control law, *Smart Materials and Struc-*
667 *tures* 28 (3) (2019) Article ID 035015. doi:10.1088/1361-665X/aafd56.
- 668 [15] X. Ma, Z. Wang, B. Zhou, S. Xue, A study on performance of distributed
669 piezoelectric composite actuators using galerkin method, *Smart Materi-*
670 *als and Structures* 28 (10) (2019) Article ID 105049. doi:10.1088/1361-
671 665X/ab3f3d.

- 672 [16] A. Baz, S. Poh, Performance of an active control system with piezoelec-
673 tric actuators, *Journal of Sound and Vibration* 126 (2) (1988) 327–343.
674 doi:10.1016/0022-460X(88)90245-3.
- 675 [17] I. Bruant, L. Gallimard, S. Nikoukar, Optimal piezoelectric actuator
676 and sensor location for active vibration control, using genetic algo-
677 rithm, *Journal of Sound and Vibration* 329 (10) (2010) 1615–1635.
678 doi:10.1016/j.jsv.2009.12.001.
- 679 [18] K. Ramesh Kumar, S. Narayanan, Active vibration control of beams with
680 optimal placement of piezoelectric sensor/actuator pairs, *Smart Materi-
681 als and Structures* 17 (5) (2008) article ID: 055008. doi:10.1088/0964-
682 1726/17/5/055008.
- 683 [19] V. Gupta, M. Sharma, N. Thakur, Optimization criteria for optimal place-
684 ment of piezoelectric sensors and actuators on a smart structure: A techni-
685 cal review, *Journal of Intelligent Material Systems and Structures* 21 (12)
686 (2010) 1227–1243. doi:10.1177/1045389X10381659.
- 687 [20] Z. Qiu, X. Zhang, H. Wu, H. Zhang, Optimal placement and
688 active vibration control for piezoelectric smart flexible cantilever
689 plate, *Journal of Sound and Vibration* 301 (3-5) (2007) 521–543.
690 doi:10.1016/j.jsv.2006.10.018.
- 691 [21] A. Belloli, P. Ermanni, Optimum placement of piezoelectric ceramic mod-
692 ules for vibration suppression of highly constrained structures, *Smart
693 Materials and Structures* 16 (5) (2007) 1662–1671. doi:10.1088/0964-
694 1726/16/5/019.
- 695 [22] W. P. Li, H. Huang, Integrated optimization of actuator placement and
696 vibration control for piezoelectric adaptive trusses, *Journal of Sound and
697 Vibration* 332 (1) (2013) 17–32. doi:10.1016/j.jsv.2012.08.005.
- 698 [23] D. Oshmarin, N. Iurlova, N. Sevodina, M. Iurlov, Algorithm for the
699 layout of a piezoelectric element in an elastic medium providing the

- 700 maximal piezoelectric effect within a specified frequency range, Inter-
701 national Journal of Smart and Nano Materials 10 (4) (2019) 268–284.
702 doi:10.1080/19475411.2019.1576070.
- 703 [24] A. Preumont, *Mechatronics: Dynamics of Electromechanical and Piezo-*
704 *electric Systems*, Springer, 2006.
- 705 [25] S. Moheimani, A. Fleming, *Piezoelectric Transducers for Vibration Control*
706 *and Damping*, Springer-Verlag, 2006.
- 707 [26] O. Thomas, J. Ducarne, J. Deü, Performance of piezoelectric shunts for
708 vibration reduction, *Smart Materials and Structures* 21 (1) (2012) Article
709 ID 015008.
- 710 [27] J. Ducarne, O. Thomas, J. Deü, Placement and dimension optimization of
711 shunted piezoelectric patches for vibration reduction, *Journal of Sound and*
712 *Vibration* 331 (14) (2012) 3286–3303.
- 713 [28] S. Chesne, C. Jean-Mistral, L. Gaudiller, Experimental identification
714 of smart material coupling effects in composite structures, *Smart Ma-*
715 *terials and Structures* 22 (2013) article ID: 075007. doi:10.1088/0964-
716 1726/22/7/075007.
- 717 [29] R. Nowak, M. Pietrzakowski, P. Rumianek, Influence of design param-
718 eters on bending piezoelectric harvester effectiveness: Static approach,
719 *Mechanical Systems and Signal Processing* 143 (2020) article ID: 106833.
720 doi:10.1016/j.ymssp.2020.106833.
- 721 [30] B. Bayik, A. Aghakhani, I. Basdogan, A. Erturk, Equivalent circuit model-
722 ing of a piezo-patch energy harvester on a thin plate with ac-dc conversion,
723 *Smart Materials and Structures* 25 (5) (2016) article ID: 055015.
- 724 [31] P. Peralta, R. Ruiz, A. Taflanidis, Bayesian identification of elec-
725 tromechanical properties in piezoelectric energy harvesters, *Mechan-*
726 *ical Systems and Signal Processing* 141 (2020) article ID: 106506.
727 doi:10.1016/j.ymssp.2019.106506.

- 728 [32] N. Hagood, A. von Flotow, Damping of structural vibrations with piezo-
729 electric materials and passive electrical networks, *Journal of Sound and*
730 *Vibration* 146 (1991) 243–268.
- 731 [33] A. Badel, G. Sebald, D. Guyomar, M. Lallart, E. Lefeuvre, C. Richard,
732 J. Qiu, Piezoelectric vibration control by synchronized switching on
733 adaptive voltage sources: Towards wideband semi-active damping, *Jour-*
734 *nal of the Acoustical Society of America* 119 (5) (2006) 2815–2825.
735 doi:10.1121/1.2184149.
- 736 [34] R. Darleux, B. Lossouarn, J.-F. Deü, Passive self-tuning inductor for
737 piezoelectric shunt damping considering temperature variations, *Journal*
738 *of Sound and Vibration* 432 (2018) 105–118.
- 739 [35] G. Caruso, A critical analysis of electric shunt circuits employed in piezo-
740 electric passive vibration damping, *Smart Materials and Structures* 10 (5)
741 (2001) 1059–1068.
- 742 [36] G. Tairidis, Vibration control of smart composite structures using shunted
743 piezoelectric systems and neuro-fuzzy techniques, *Journal of Vibration and*
744 *Control* 25 (18) (2019) 2397–2408.
- 745 [37] P. Gardonio, D. Casagrande, Shunted piezoelectric patch vibration ab-
746 sorber on two-dimensional thin structure: tuning considerations, *Journal*
747 *of Sound and Vibration* 395 (2017) 26–47.
- 748 [38] V. Matveenko, N. Iurlova, D. Oshmarin, N. Sevodina, M. Iurlov, An ap-
749 proach to determination of shunt circuits parameters for damping vibra-
750 tions, *International Journal of Smart and Nano Materials* 9 (2) (2018) 135–
751 149.
- 752 [39] U. Andreaus, M. Porfiri, Effect of electrical uncertainties on resonant piezo-
753 electric shunting, *Journal of Intelligent Material Systems and Structures* 18
754 (2007) 477–485.

- 755 [40] J. Høgsberg, S. Krenk, Balanced calibration of resonant shunt circuits for
756 piezoelectric vibration control, *Journal of Intelligent Material Systems and*
757 *Structures* 23 (17) (2012) 1937–1948.
- 758 [41] J. Høgsberg, S. Krenk, Balanced calibration of resonant piezoelectric rl
759 shunts with quasi-static background flexibility correction, *Journal of Sound*
760 *and Vibration* 341 (2015) 16–30.
- 761 [42] P. Soltani, G. Kerschen, G. Tondreau, A. Deraemaeker, Tuning of a piezo-
762 electric vibration absorber attached to a damped structure, *Journal of In-*
763 *telligent Material Systems and Structures* 28 (9) (2017) 1115–1129.
- 764 [43] K. Yamada, H. Matsuhisa, H. Utsuno, K. Sawada, Optimum tuning of se-
765 ries and parallel lr circuits for passive vibration suppression using piezoelec-
766 tric elements, *Journal of Sound and Vibration* 329 (24) (2010) 5036–5057.
- 767 [44] S.-Y. Wu, Method for multiple mode piezoelectric shunting with single pzt
768 transducer for vibration control, *Journal of Intelligent Material Systems*
769 *and Structures* 9 (1998) 991–998.
- 770 [45] S. Behrens, S. Moheimani, A. Fleming, Multiple mode current flowing pas-
771 sive piezoelectric shunt controller, *Journal of Sound and Vibration* 266 (5)
772 (2003) 929–942. doi:10.1016/S0022-460X(02)01380-9.
- 773 [46] A. J. Fleming, S. Behrens, S. O. R. Moheimani, Reducing the Inductance
774 Requirements of Piezoelectric Shunt Damping Systems, *Smart Materials*
775 *and Structures* 12 (1) (2003) 57–64. doi:10.1088/0964-1726/12/1/307.
- 776 [47] G. Raze, A. Paknejad, G. Zhao, C. Collette, G. Kerschen, Multi-
777 modal vibration damping using a simplified current blocking shunt cir-
778 cuit, *Journal of Intelligent Material Systems and Structures* in press.
779 doi:10.1177/1045389X20930103.
- 780 [48] S. Behrens, A. J. Fleming, S. O. R. Moheimani, A broadband controller for
781 shunt piezoelectric damping of structural vibration, *Smart Materials and*
782 *Structures* 12 (1) (2003) 18–28.

- 783 [49] B. S. Beck, K. A. Cunefare, M. Collet, The power output and efficiency
784 of a negative capacitance shunt for vibration control of a flexural system,
785 Smart Materials and Structures 22 (6), article ID 065009.
- 786 [50] G. Raze, B. Lossouarn, A. Paknejad, G. Zhao, J.-F. Deü, C. Collette,
787 G. Kerschen, A multimodal nonlinear piezoelectric vibration absorber, in:
788 Proceedings of the International Conference on Noise and Vibration Engi-
789 neering ISMA and International Conference on Uncertainty in Structural
790 Dynamics USD - September 17-19, 2018 - Leuven (Belgium), 2018.
- 791 [51] G. Raze, A. Jadoul, S. Guichaux, V. Broun, G. Kerschen, A digital nonlin-
792 ear piezoelectric tuned vibration absorber, Smart Materials and Structures
793 29 (1) (2020) article ID: 015007. doi:10.1088/1361-665X/ab5176.
- 794 [52] C. Bricault, C. Pézerat, M. Collet, A. Pyskir, P. Perrard, G. Matten,
795 V. Romero-Garcia, Multimodal reduction of acoustic radiation of thin
796 plates by using a single piezoelectric patch with a negative capacitance
797 shunt, Applied Acoustics 145 (2019) 320–327.
- 798 [53] Y. Fan, M. Collet, M. Ichchou, L. Li, O. Bareille, Z. Dimitrijevic, A
799 wave-based design of semi-active piezoelectric composites for broadband
800 vibration control, Smart Materials and Structures 25 (5) (2016) article ID:
801 055032. doi:10.1088/0964-1726/25/5/055032.
- 802 [54] R. Darleux, B. Lossouarn, J.-F. Deü, Broadband vibration damping of non-
803 periodic plates by piezoelectric coupling to their electrical analogues, Smart
804 Materials and Structures 29 (2020) article ID: 054001.
- 805 [55] F. Xie, Y. Su, W. Zhou, W.-Z. Zhang, Design and evaluation of a shunted
806 flexible piezoelectric damper for vibration control of cable structures, Smart
807 Materials and Structures 28 (8) (2019) article ID. 085031. doi:10.1088/1361-
808 665X/ab2c14.
- 809 [56] K. Billon, N. Montcoudiol, A. Aubry, R. Pascual, F. Mosca, F. Jean,
810 C. Pezerat, C. Bricault, S. Chesné, Vibration isolation and damping using

- 811 a piezoelectric flextensional suspension with a negative capacitance shunt,
812 Mechanical Systems and Signal Processing 140 (2020) article ID: 106696.
813 doi:10.1016/j.ymssp.2020.106696.
- 814 [57] W. Tang, L.-B. Wang, Y.-M. Ren, B. Bao, J.-J. Cao, Design and exper-
815 imental analysis of self-sensing ssdnc technique for semi-active vibration
816 control, Smart Materials and Structures 27 (8) (2018) Article ID 085028.
817 doi:10.1088/1361-665X/aad0b9.
- 818 [58] H. Asanuma, T. Komatsuzaki, Nonlinear piezoelectricity and damping
819 in partially-covered piezoelectric cantilever with self-sensing synchronized
820 switch damping on inductor circuit, Mechanical Systems and Signal Pro-
821 cessing 144 (2020) article ID: 106867. doi:10.1016/j.ymssp.2020.106867.
- 822 [59] L. Yan, B. Bao, D. Guyomar, M. Lallart, Periodic structure
823 with interconnected nonlinear electrical networks, Journal of In-
824 telligent Material Systems and Structures 28 (2) (2017) 204–229.
825 doi:10.1177/1045389X16649448.
- 826 [60] M. Berardengo, O. Thomas, C. Giraud-Audine, S. Manzoni, Improved re-
827 sistive shunt by means of negative capacitance: new circuit, performances
828 and multi mode control, Smart Materials and Structures 25 (2016) Article
829 ID 075033.
- 830 [61] B. de Marneffe, A. Preumont, Vibration damping with negative capacitance
831 shunts: theory and experiment, Smart Materials And Structures 17 (3)
832 (2008) Article ID 035015.
- 833 [62] J. Høgsberg, S. Krenk, Calibration of piezoelectric rl shunts with explicit
834 residual mode correction, Journal of Sound and Vibration 386 (2017) 65–81.
- 835 [63] M. Berardengo, S. Manzoni, A. Conti, Multi-mode passive piezoelectric
836 shunt damping by means of matrix inequalities, Journal of Sound and Vi-
837 bration 405 (2017) 287–305.

- 838 [64] M. Berardengo, S. Manzoni, O. Thomas, M. Vanali, Piezoelectric resonant
839 shunt enhancement by negative capacitances: optimisation, performance
840 and resonance cancellation, *Journal of Intelligent Material Systems and*
841 *Structures* 29 (12) (2018) 2581–2606.
- 842 [65] J. Toftekær, J. Høgsberg, Multi-mode piezoelectric shunt damping with
843 residual mode correction by evaluation of modal charge and voltage, *Jour-*
844 *nal of Intelligent Material Systems and Structures* 31 (4) (2019) 570–586.
- 845 [66] O. Thomas, J.-F. Deü, J. Ducarne, Vibration of an elastic structure with
846 shunted piezoelectric patches: efficient finite-element formulation and elec-
847 tromechanical coupling coefficients, *International Journal of Numerical*
848 *Methods in Engineering* 80 (2) (2009) 235–268.
- 849 [67] J. Høgsberg, Consistent frequency-matching calibration procedure for elec-
850 tromechanical shunt absorbers, *Journal of Vibration and Control* 26 (13-14)
851 (2020) 1133–1144.
- 852 [68] J. S. Hwang, H. Kim, J. Kim, Estimation of the modal mass of a struc-
853 ture with a tuned-mass damper using H-infinity optimal model reduction,
854 *Engineering Structures* 28 (1) (2006) 34–42.
- 855 [69] Evaluation of measurement data - guide to the expression of uncertainty in
856 measurement, 2008, JCGM 100:2008.
- 857 [70] O. Thomas, C. Touzé, A. Chaigne, Asymmetric non-linear forced vibrations
858 of free-edge circular plates. part ii: experiments, *Journal of Sound and*
859 *Vibration* 265 (5) (2003) 1075–1101.
- 860 [71] L. von Wangeheim, Modification of the classical gic structure and its ap-
861 plication to rc-oscillators, *Electronics Letters* 32 (1) (1996) 6–8.
- 862 [72] H. Van der Auweraer, P. Guillaume, P. Verboven, S. Vanlanduit, Applica-
863 tion of a fast-stabilizing frequency domain parameter estimation method,
864 *Journal of Dynamic Systems, Measurement and Control, Transactions of*
865 *the ASME* 123 (4) (2001) 651–658. doi:10.1115/1.1410369.